University of Nebraska - Lincoln
DigitalCommons@University of Nebraska - Lincoln

Evgeny Tsymbal Publications | Research Papers in Physics and Astronomy

11-11-2017

Epitaxial thin films of Dirac semimetal antiperovskite Cu_3PdN

C. X. Quintela
University of Wisconsin-Madison

N. Campbell
University of Wisconsin - Madison

D. F. Shao
University of Nebraska - Lincoln, dfshao@unl.edu

J. Irwin
University of Wisconsin-Madison

D. T. Harris
University of Wisconsin - Madison

See next page for additional authors

Follow this and additional works at: http://digitalcommons.unl.edu/physicstsymbal

 Part of the Condensed Matter Physics Commons

Quintela, C. X.; Campbell, N.; Shao, D. F.; Irwin, J.; Harris, D. T.; Lie, L.; Anderson, T. J.; Reiser, N.; Pan, X. Q.; Tsymbal, Evgeny Y.; Rzchowski, M. S.; and Eom, C B., "Epitaxial thin films of Dirac semimetal antiperovskite Cu_3PdN" (2017). *Evgeny Tsymbal Publications*. 85.
http://digitalcommons.unl.edu/physicstsymbal/85

This Article is brought to you for free and open access by the Research Papers in Physics and Astronomy at DigitalCommons@University of Nebraska - Lincoln. It has been accepted for inclusion in Evgeny Tsymbal Publications by an authorized administrator of DigitalCommons@University of Nebraska - Lincoln.

Authors
C. X. Quintela, N. Campbell, D. F. Shao, J. Irwin, D. T. Harris, L. Lie, T. J. Anderson, N. Reiser, X. Q. Pan, Evgeny Y. Tsymbal, M. S. Rzchowski, and C B. Eom

This article is available at DigitalCommons@University of Nebraska - Lincoln: http://digitalcommons.unl.edu/physicstsymbal/85

Epitaxial thin films of Dirac semimetal antiperovskite Cu_3PdN

C. X. Quintela, N. Campbell, D. F. Shao, J. Irwin, D. T. Harris, L. Xie, T. J. Anderson, N. Reiser, X. Q. Pan, E. Y. Tsymbal, M. S. Rzchowski, and C. B. Eom

Citation: APL Materials **5**, 096103 (2017); doi: 10.1063/1.4992006
View online: https://doi.org/10.1063/1.4992006
View Table of Contents: http://aip.scitation.org/toc/apm/5/9
Published by the American Institute of Physics

Articles you may be interested in

Heteroepitaxial growth of tetragonal $Mn_{2.7-x}Fe_xGa_{1.3}$ ($0 \leq x \leq 1.2$) Heusler films with perpendicular magnetic anisotropy
APL Materials **5**, 096102 (2017); 10.1063/1.4991468

Interfacial B-site atomic configuration in polar (111) and non-polar (001) $SrIrO_3/SrTiO_3$ heterostructures
APL Materials **5**, 096110 (2017); 10.1063/1.4993170

Growth of strontium ruthenate films by hybrid molecular beam epitaxy
APL Materials **5**, 096101 (2017); 10.1063/1.4998772

Exposing high-energy surfaces by rapid-anneal solid phase epitaxy
APL Materials **5**, 086103 (2017); 10.1063/1.4992004

Reduction of in-plane field required for spin-orbit torque magnetization reversal by insertion of Au spacer in Pt/Au/Co/Ni/Co/Ta
APL Materials **5**, 106104 (2017); 10.1063/1.4991950

Mapping cation diffusion through lattice defects in epitaxial oxide thin films on the water-soluble buffer layer $Sr_3Al_2O_6$ using atomic resolution electron microscopy
APL Materials **5**, 096108 (2017); 10.1063/1.4994538

Epitaxial thin films of Dirac semimetal antiperovskite Cu_3PdN

C. X. Quintela,[1] N. Campbell,[2] D. F. Shao,[3] J. Irwin,[2] D. T. Harris,[1] L. Xie,[4] T. J. Anderson,[1] N. Reiser,[2] X. Q. Pan,[5] E. Y. Tsymbal,[3] M. S. Rzchowski,[2] and C. B. Eom[1,a]

[1]*Department of Materials Science and Engineering, University of Wisconsin-Madison, Madison, Wisconsin 53706, USA*
[2]*Department of Physics, University of Wisconsin-Madison, Madison, Wisconsin 53706, USA*
[3]*Department of Physics and Astronomy and Nebraska Center for Materials and Nanoscience, University of Nebraska, Lincoln, Nebraska 68588, USA*
[4]*National Laboratory of Solid State Microstructures and College of Engineering and Applied Sciences, Nanjing University, Nanjing, Jiangsu 210093, People's Republic of China*
[5]*Department of Chemical Engineering and Materials Science, University of California Irvine, Irvine, California 92697, USA*

(Received 25 June 2017; accepted 28 August 2017; published online 11 September 2017)

The growth and study of materials showing novel topological states of matter is one of the frontiers in condensed matter physics. Among this class of materials, the nitride antiperovskite Cu_3PdN has been proposed as a new three-dimensional Dirac semimetal. However, the experimental realization of Cu_3PdN and the consequent study of its electronic properties have been hindered due to the difficulty of synthesizing this material. In this study, we report fabrication and both structural and transport characterization of epitaxial Cu_3PdN thin films grown on (001)-oriented $SrTiO_3$ substrates by reactive magnetron sputtering and post-annealed in NH_3 atmosphere. The structural properties of the films, investigated by x-ray diffraction and scanning transmission electron microscopy, establish single phase Cu_3PdN exhibiting cube-on-cube epitaxy (001)[100]Cu_3PdN||(001)[100]$SrTiO_3$. Electrical transport measurements of as-grown samples show metallic conduction with a small temperature coefficient of the resistivity of 1.5×10^{-4} K^{-1} and a positive Hall coefficient. Post-annealing in NH_3 results in the reduction of the electrical resistivity accompanied by the Hall coefficient sign reversal. Using a combination of chemical composition analyses and *ab initio* band structure calculations, we discuss the interplay between nitrogen stoichiometry and magneto-transport results in the framework of the electronic band structure of Cu_3PdN. Our successful growth of thin films of antiperovskite Cu_3PdN opens the path to further investigate its physical properties and their dependence on dimensionality, strain engineering, and doping. © *2017 Author(s). All article content, except where otherwise noted, is licensed under a Creative Commons Attribution (CC BY) license (http://creativecommons.org/licenses/by/4.0/).* [http://dx.doi.org/10.1063/1.4992006]

The discovery of three-dimensional (3D) Dirac semimetal (DSM) phases in Na_3Bi[1,2] and Cd_3As_2[3–7] was a breakthrough in condensed matter physics as it launched the growth and study of 3D topological materials. Bulk 3D-DSMs, characterized by having Dirac-type energy dispersion in the 3D momentum $\boldsymbol{k}$-space close to the Fermi level,[8] are usually viewed as bulk counterparts of graphene owing to their similar electronic structure and unique transport properties, including ultrahigh electron motility and giant magnetoresistance.[6,7] Moreover, Dirac nodes in bulk 3D-DSMs are robust against physical perturbations and doping as they are protected by distinct crystal symmetries.[3,8,9] In addition to their unique physical properties and potential electronic applications,[2,10] 3D-DSMs are also a platform to realize other topological phases of interest, such as

[a]Author to whom correspondence should be addressed: eom@engr.wisc.edu

 © Author(s) 2017

topological insulators, topological superconductors, 3D Weyl semimetals, or node-line semimetals (NLSs).[2,11–13]

Recently, two groups independently proposed nitride antiperovskite Cu_3PdN as a new 3D-DSM material with three pairs of Dirac points stabilized by the C_4 rotational crystal symmetry of Cu_3PdN.[14,15] A schematic diagram of the proposed electronic band structure of Cu_3PdN near the Fermi level (E_F) is shown in Fig. 1(a), comprising a normal quadratic conduction band at the gamma (Γ) point, a linear dispersive valence band crossing E_F along the R-X momentum direction, and a Dirac cone located along the R-M direction. In the absence of spin-orbit coupling (SOC), the gap at the R-X direction closes and calculations predict Cu_3PdN to be a NLS, another topologically non-trivial phase in which the linear dispersive bands meet along a line in the ***k***-space (node-line) instead of at discrete Dirac points. Experimentally, this phase can be achieved by replacing Pd by lighter atoms like Zn. In the NLS phase, "drumhead" surface states are predicted, which have been proposed as a platform for achieving high-temperature superconductivity.[16–19] Additionally, if the C_4 crystal symmetry of Cu_3PdN is broken, the Dirac nodes in the 3D-DSM phase are gapped and Cu_3PdN becomes a strong topological insulator.[14,15]

Despite its intriguing predicted physical properties, the experimental realization of bulk Cu_3PdN and its consequent electronic and transport characterization has been hindered due to the difficulty of synthesizing this material. The fact that Cu_3PdN decomposes at 470 °C,[20] together with the inherent unreactive nature of most nitrogen sources below that temperature,[21,22] makes fabrication of this compound challenging. Low-temperature solution synthesis has been used to fabricate nanoparticles of Cu_3PdN,[23,24] but the small size and polycrystalline nature of the nanoparticles hamper the study of the intrinsic electronic properties of Cu_3PdN. Fabrication of micrometric crystals was reported using high pressure synthesis techniques;[20] however, as with the solution derived material, the microscopic size makes electronic characterization challenging.

In this letter, we report fabrication of epitaxial thin films of Cu_3PdN on (001)-oriented $SrTiO_3$ single crystal substrates. We overcame the difficulty introduced by low-temperature synthesis by using reactive magnetron sputtering, a deposition technique that can produce metal nitrides at relatively low temperatures by ionizing N_2 gas during the growth.[25] Our structural analyses confirm single phase Cu_3PdN films exhibiting cube-on-cube epitaxy on $SrTiO_3$. We show that post-annealing in NH_3 results in the reduction of the electrical resistivity of the films accompanied by the Hall coefficient sign reversal from positive to negative. Using secondary ion mass spectrometry (SIMS) compositional analysis and *ab initio* band structure calculations, we discuss the interplay between nitrogen stoichiometry and magneto-transport results in the framework of the electronic structure of Cu_3PdN.

In Fig. 1(b), we show the crystallographic unit cell of Cu_3PdN. Ideal Cu_3PdN has a cubic perovskite-type crystal structure (space group *Pm-3m*) with reported bulk lattice constant $a = 3.854$ Å for nearly stoichiometric $Cu_3Pd_{0.989}N$ single crystals.[20] In antiperovskite Cu_3PdN, nitrogen is located

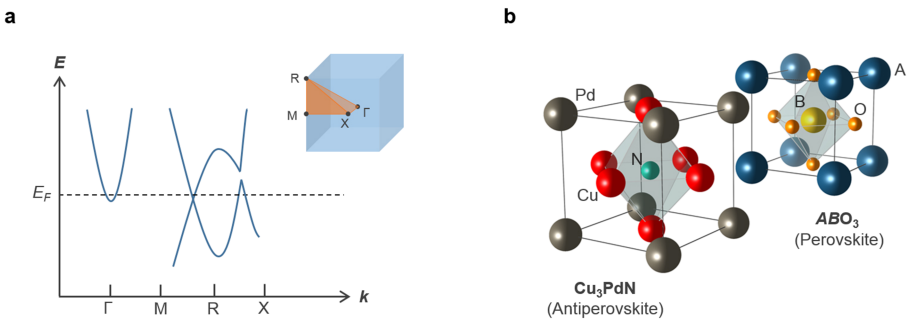

FIG. 1. (a) Schematic of the first Brillouin zone and reduced electronic band structure near the Fermi level (E_F) for bulk Cu_3PdN considering spin-orbit coupling. A Dirac node is located along the M-R momentum direction, a linear dispersive valence band crossing E_F along the R-X direction, and an electron pocked at the Γ point. (b) Perspective view of the unit cells of ideal cubic antiperovskite Cu_3PdN and ABO_3 oxide perovskite showing their geometrically identical crystal structures (space group *Pm-3m*).

at the center of the unit cell in an octahedral interstitial surrounded by Cu atoms (face-centered) and Pd atoms at the corners of the cubic unit cell. A relevant feature of the crystal structure of Cu_3PdN is its good structural and lattice match with most of the single-crystal oxide perovskite substrates with a general chemical formula ABO_3, as shown in Fig. 1(b). In terms of thin-film growth, these similarities between film and substrate are desirable as they are basic criteria to promote epitaxial growth.

Under the previous criterion, we chose (001) $SrTiO_3$ single crystals as substrates to grow Cu_3PdN as they not only have similar crystal structures (same *Pm-3m* space group) but also have a good lattice match of $\varepsilon = 1.3\%$ in the (001) plane.[26] Moreover, (001)-oriented $SrTiO_3$ substrates can be treated by using a buffered-HF etch and subsequent high-temperature annealing to obtain atomically-flat, TiO_2-terminated surfaces.[27] Our Cu_3PdN films were grown by DC reactive planar magnetron sputtering using a Cu_3Pd stoichiometric target (99.9% purity) in an Ar (20 sccm)/N_2 (20 sccm) atmosphere of 15 mTorr. The target was sputtered at 50 W and the heater temperature was set at 330 °C. Prior to deposition, a base pressure of 1×10^{-7} Torr was achieved. We found the window of optimum growth conditions to obtain epitaxial and single phase Cu_3PdN to be extremely narrow: slight deviations from the ideal conditions result in polycrystalline Cu_3PdN and/or the emergence of other phases. The as-grown films were then post-annealed in flowing NH_3 (99.99%) atmosphere at 330 °C in a tubular furnace to investigate the effect of annealing on the structural, compositional, and electrical properties of the films. Both as-grown and annealed Cu_3PdN films are stable in air and resistant to common solvents like acetone, ethanol, or isopropyl alcohol. The results presented in this study correspond to 60 nm thick films (labeled as as-grown) that were subsequently post-annealed in NH_3 for a total time of 36 h (labeled as annealed).

The structural properties of both as-grown and annealed films were investigated at room temperature by XRD using a four-circle X-ray diffractometer equipped with Cu–Kα_1 radiation. In Fig. 2(a), we show a characteristic XRD out-of-plane 2θ scan for as-grown and annealed Cu_3PdN. For both films, only the (00*l*) reflections of Cu_3PdN and $SrTiO_3$ are observed, indicating single-phase

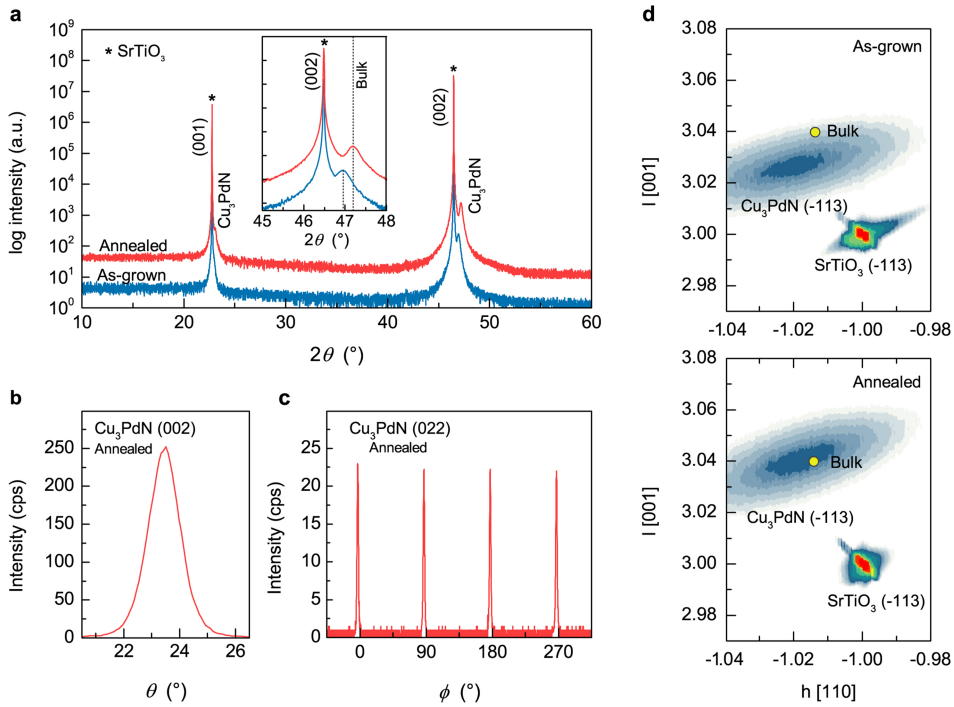

FIG. 2. (a) Out-of-plane XRD scan for both as-grown and NH_3 post-annealed Cu_3PdN films. The inset shows a magnification of the XRD scan around the $SrTiO_3$ (002) diffraction peak. (b) Rocking curve around the (002) diffraction peak for annealed Cu_3PdN. (c) ϕ-scan around the (022) peak of annealed Cu_3PdN. (d) Reciprocal space maps for as-grown and annealed Cu_3PdN around the (−113) reflection.

(00*l*)-oriented Cu_3PdN. In Fig. 2(b), we show a XRD rocking curve evaluated at the (002) reflection for annealed Cu_3PdN, which shows a full-width at half-maximum (FWHM) of 1.32°. The in-plane epitaxial arrangement of the films was confirmed by off-axis azimuthal ϕ-scans of the (022) reflection. A representative ϕ-scan for annealed Cu_3PdN is shown in Fig. 2(c). The scan shows four diffraction peaks located 90° apart at identical azimuthal angles as the $SrTiO_3$ substrate, confirming cube-on-cube epitaxial growth with $[100]Cu_3PdN \| [100]SrTiO_3$ relationship.

Now we focus on the effect of NH_3 annealing on the structural properties of the films. In the inset of Fig. 2(a), we show a 2θ scan around the $SrTiO_3$ (002) peak, where it is seen that post-annealing in NH_3 results in a shift of the Cu_3PdN (002) peak toward the 2θ value previously reported for bulk $Cu_3Pd_{0.989}N$ single crystals.[19] This result is in agreement with X-ray reciprocal space mapping (RSM) measurements taken around the (−113) reciprocal lattice point [Fig. 2(d)], which shows that post-annealing in NH_3 drives the Cu_3PdN (−113) peak towards a nearly relaxed, bulk-like, state. The in-plane ($a_{\|}$) and out-of-plane ($a_{\perp}$) lattice constants were determined to be $a_{\|} \approx 3.83 \pm 0.01$ Å and $a_{\perp} \approx 3.87 \pm 0.01$ Å for the as-grown sample and $a_{\|} \approx 3.84 \pm 0.01$ Å and $a_{\perp} \approx 3.85 \pm 0.01$ Å for the annealed one, which indicates that the shift of the (−113) peak is accompanied with a slight variation of the unit cell volume toward the bulk value. As expected from the low annealing temperature of 330 °C, as-grown and annealed films show insignificant changes in the FWHM values of 2θ, rocking curve, and off-axis peaks, indicating limited changes to the crystallite size and mosaic spread. In order to investigate the effect of possible chemical compositional changes on the structural properties of the films after the post-annealing treatment, we performed the depth profile SIMS analysis.[28] The results show an average of ∼10% lower nitrogen concentration in the annealed sample compared to the as-grown one (Fig. S1 of the supplementary material). NH_3 annealing generally increases the nitrogen content of nitrides;[29] however, the low decomposition temperature of Cu_3PdN limits the annealing temperature below the decomposition temperature of NH_3,[30] where a limited nitrogen activity is expected.

We investigated the surface morphology and microstructure of the films by using atomic force microscopy (AFM) and cross-sectional scanning transmission electron microscopy (STEM), respectively. Figure 3(a) shows an AFM image for as-grown Cu_3PdN films with a typical root mean square surface roughness of ∼1 nm. Similar surface morphology was observed in annealed samples, which is a further indication that low-temperature annealing in NH_3 does not produce visible changes to the crystallite size. The presence of surface grains indicates the columnar grain growth mode during the deposition. This is consistent with cross-sectional STEM analyses, which reveal a columnar grain structure with (001)-oriented grains of ∼40–50 nm in diameter. The columnar growth mode is usually associated with low surface mobility of incoming atoms during deposition,[31] which in our case could be related to the limitation of low-temperature growth required to obtain single-phase epitaxial Cu_3PdN films. A low magnification STEM image showing the Cu_3PdN film and the top of the $SrTiO_3$ substrate is shown in Fig. 3(b). At the interface with the $SrTiO_3$ substrate, the Cu_3PdN lattice shows some crystallographic defects, including antiphase domains and dislocations. Away

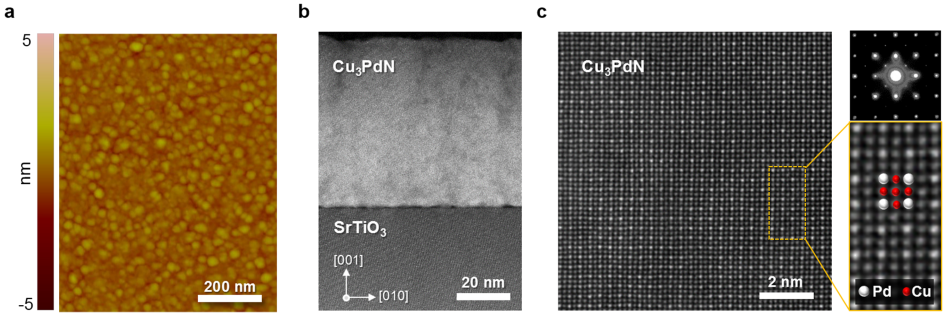

FIG. 3. (a) Characteristic AFM image of Cu_3PdN thin films. (b) Low magnification STEM image showing the Cu_3PdN film and the top of the $SrTiO_3$ substrate. (c) Atomic resolution STEM-HAADF image away from the interface. On the right, we show a selected area electron diffraction (SAED) pattern obtained in this region (top) and an enlarged region of the image including the [100] projected Cu_3PdN unit cell (bottom).

from the interface, the crystalline quality of Cu_3PdN substantially improves, as shown in the atomic resolution STEM high-angle annular dark field (HAADF) image in Fig. 3(c) and the corresponding fast Fourier transformation (FFT) pattern.

We now turn to the magneto-transport characterization of the films, performed using the van der Pauw configuration in a liquid-helium cryostat equipped with a 1.5 T magnet. Figures 4(a) and 4(b) show typical temperature dependence of the resistivity (ρ) for both as-grown and annealed films. Upon cooling from room temperature, the electrical resistivity for both samples decreases monotonically down to 20 K, exhibiting metallic behavior as predicted by theory.[32–34] The variation of ρ in this temperature range is very small, resulting in a low temperature coefficient of resistivity (TCR = $d\rho/(\rho_0 dT)$, where ρ_0 is the resistivity at 300 K) of 1.5×10^{-4} K^{-1}. Below 20 K, both samples show a small up-turn in the resistivity. Although $\rho(T)$ for both as-grown and annealed films show similar trends, annealed samples show a noticeable reduction of the resistivity of ~30%. Furthermore, this resistivity decrease is accompanied by the Hall coefficient (R_H) sign reversal from positive (as-grown) to negative (annealed), as we show in Fig. 4(c). We found that both the R_H sign reversal and ρ change are dependent on annealing time: as seen in Figs. 4(e) and 4(f), increasing the annealing time results in a gradual decrease of ρ and concomitant change of R_H from positive to negative. Furthermore, the changes in ρ and R_H are correlated with the variation of $a_\perp$ with annealing time [Fig. 4(d)]. The fact that all ρ, R_H, and $a_\perp$ show a similar dependence with annealing time indicates a correlation between electronic properties and nitrogen stoichiometry.

We next discuss the R_H sign reversal in the framework of the electronic band structure of Cu_3PdN. As previously shown in Fig. 1(a), the electronic band structure of Cu_3PdN includes hole and electron-like bands near the Fermi level, so the magneto-transport analysis (R_H sign reversal) requires considering multiple bands. In a simplified two-band model, the Hall resistivity (ρ_{xy}) is described by the following equation:[35]

$$\rho_{xy} = \frac{\left(p\mu_h^2 - n\mu_e^2\right) B + \mu_h^2 \mu_e^2 (p-n) B^3}{|e|\left[(p\mu_h + n\mu_e)^2 + \mu_h^2 \mu_e^2 (p-n)^2 B^2\right]}, \tag{1}$$

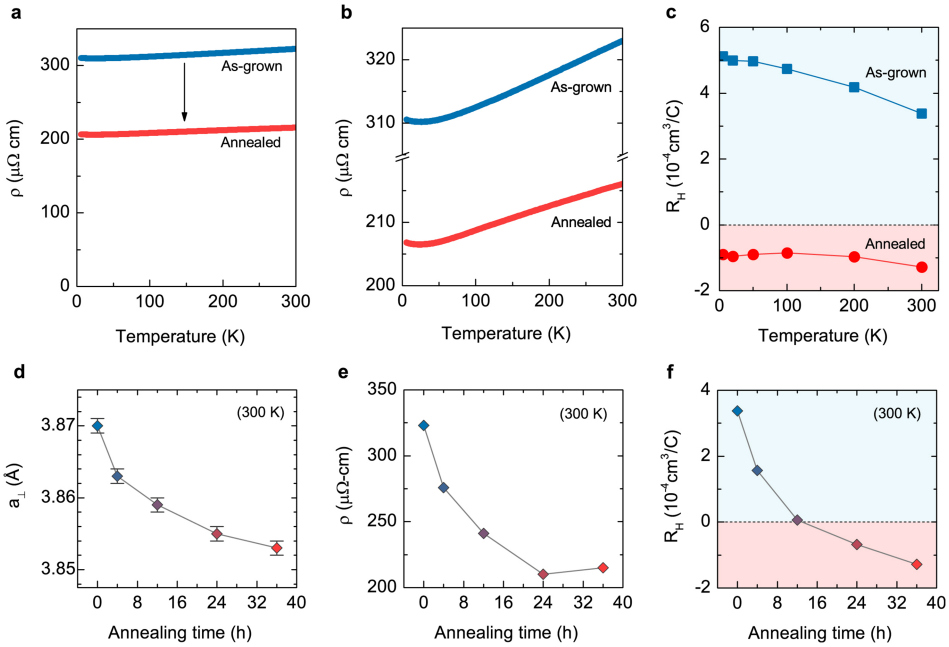

FIG. 4. (a) Resistivity (ρ) versus temperature data for as-grown and NH_3 post-annealed Cu_3PdN thin films showing a remarkably flat temperature dependence from 5 K to 300 K. (b) Zoom of the resistivity data: metallic conduction is observed from 20 K to 300 K with a small upturn at below 20 K. (c) The Hall coefficient (R_H) versus temperature for as-grown and annealed Cu_3PdN. (d)–(f) show the variation of $a_\perp$, ρ, and R_H and with annealing time (data taken at 300 K).

where B is the magnetic field, e is the electron charge, and n, p, μ_e, and μ_h are the electron and hole densities and mobilities. For nearly compensated materials ($n \approx p$) in the limit of low magnetic fields, ρ_{xy} is linearly proportional to B[36] as

$$\rho_{xy} = \frac{(p\mu_h^2 - n\mu_e^2)}{|e|(p\mu_h + n\mu_e)^2} B = R_H B \tag{2}$$

in good agreement with our experimental observations (Fig. S2 of the supplementary material). In this scenario, the magnitude and sign of R_H dramatically depend on the relative values of n, p, μ_e, and μ_h. A gradual change from positive to negative R_H, such as that observed in our Cu_3PdN films, indicates a transition from $p{\mu_h}^2 > n{\mu_e}^2$ to $p{\mu_h}^2 < n{\mu_e}^2$. Based on our SIMS chemical analyses, this transition likely arises from a variation in the carrier concentration driven by a variation in the nitrogen stoichiometry of Cu_3PdN when annealing in NH_3.

To understand the influence of nitrogen stoichiometry on the electronic properties of Cu_3PdN, we performed *ab initio* band-structure calculations using Quantum ESPRESSO package[37] with ultrasoft pseudopotentials including SOC. Exchange and correlation effects were treated within the generalized gradient approximation (GGA).[38] We used a plane-wave cutoff energy of 40 Ry and a $16 \times 16 \times 16$ $\boldsymbol{k}$-point mesh in the irreducible Brillouin zone. To simulate the nitrogen deficiency, we uniformly replaced nitrogen atoms with virtual atoms, which have fewer valence electrons than nitrogen, using the virtual crystal approximation (VCA).[39] This approach is motivated by previous theoretical studies of the C- and N-deficient metallic antiperovskites Ni_3AlC_x[40] and Mn_3AlN_x,[41] which demonstrated that the major role of C or N deficiency is to decrease the number of valence electrons and lower E_F. Figure 5(a) shows the calculated band structure of stoichiometric cubic Cu_3PdN which is in good agreement with the band structures reported in Refs. 14 and 15, revealing a Dirac node along the R-M direction, a nearly linear dispersive hole-like band along the R-X direction, and an electron pocket at the Γ point. Since nitrogen deficiency is a common source of non-stoichiometry in nitride antiperovskites,[42] it is likely that our as-grown Cu_3PdN films are slightly nitrogen deficient. Calculations for $Cu_3PdN_{0.98}$ show that E_F lies below the Dirac point, which opens two hole pockets located along the M-R and R-X symmetry lines, as indicated in Fig. 5(b). These hole pockets may be responsible for the p-type conduction and positive R_H observed experimentally in the as-grown films. Further decrease in the nitrogen content results in a gradual lowering of E_F. As an example, Fig. 5(c) shows that in $Cu_3PdN_{0.9}$, the E_F shifts closer to the bottom of the two free-electron-like bands with minima located at the M and R points. This opens two electron pockets which contribute to n-type conduction and may be responsible for the sign change of R_H observed experimentally in our annealed films. Additionally, as recently proposed,[43] small lattice constant variations due to strain could also

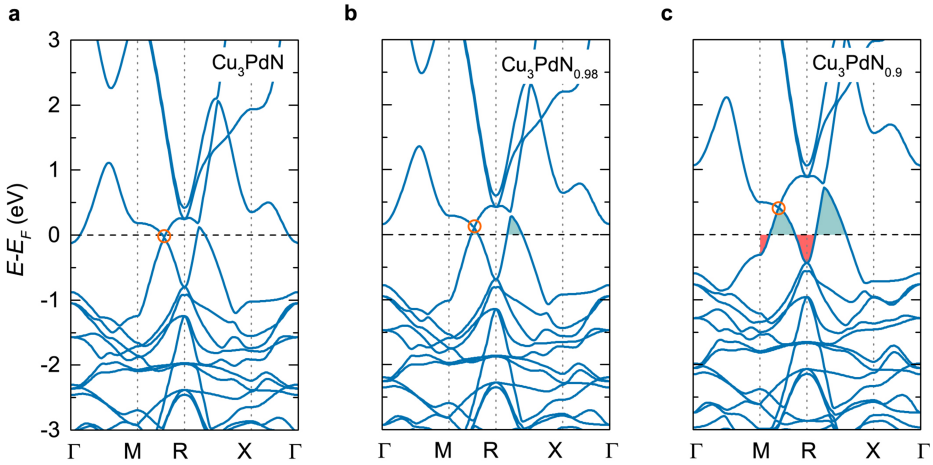

FIG. 5. Electronic band structure for cubic stoichiometric Cu_3PdN (a) and nitrogen deficient $Cu_3PdN_{0.98}$ (b) and $Cu_3PdN_{0.9}$ (c). Orange circles indicate the position of the Dirac node. Light blue areas show hole pockets and red areas electron pockets.

modify the band structure of Cu_3PdN, so a more complex scenario combining the effects of strain and nitrogen content could also explain our experimental magneto-transport results.

In conclusion, we have demonstrated the growth of epitaxial thin films of nitride antiperovskite Cu_3PdN, which is the vital first step to unlock its intrinsic physical properties. We show that Cu_3PdN is a metallic conductor, as predicted by theory, and that the magneto-transport properties depend on small variations in the nitrogen content. *Ab initio* band structure calculations show that nitrogen understoichiometry results in a decrease of the Fermi level below the Dirac node. In this context, future research should focus on investigating chemical doping as a possible tool to tune the Femi level around the Dirac node to access the predicted topological properties of Cu_3PdN. Additionally, given the good lattice match of Cu_3PdN with most of the commonly used oxide perovskite substrates, we anticipate thin film engineering to be a versatile playground to further investigate the electronic properties of Cu_3PdN under epitaxial strain, reduced dimensionality, and at interfaces with other materials.

See supplementary material for SIMS chemical composition analysis and supplementary magneto-transport data.

This work was supported by the National Science Foundation under DMREF Grant No. DMR-1629270. Research at the University of Nebraska-Lincoln was partly supported by the NSF MRSEC (Grant No. DMR-1420645). The work at Nanjing University was supported by the National Natural Science Foundation of China (No. 51302132).

[1] Z. J. Wang, Y. Sun, X. Q. Chen, C. Franchini, G. Xu, H. M. Weng, X. Dai, and Z. Fang, "Dirac semimetal and topological phase transitions in A_3Bi (A = Na, K, Rb)," Phys. Rev. B **85**, 195320 (2012).
[2] Z. K. Liu, B. Zhou, Y. Zhang, Z. J. Wang, H. M. Weng, D. Prabhakaran, S.-K. Mo, Z. X. Shen, Z. Fang, X. Dai, Z. Hussain, and Y. L. Chen, "Discovery of a three-dimensional topological Dirac semimetal, Na_3Bi," Science **343**, 864 (2014).
[3] Z. J. Wang, H. M. Weng, Q. S. Wu, X. Dai, and Z. Fang, "Three-dimensional Dirac semimetal and quantum transport in Cd_3As_2," Phys. Rev. B **88**, 125427 (2013).
[4] Z. K. Liu, J. Jiang, B. Zhou, Z. J. Wang, Y. Zhang, H. M. Weng, D. Prabhakaran, S.-K. Mo, H. Peng, P. Dudin, T. Kim, M. Hoesch, Z. Fang, X. Dai, Z. X. Shen, D. L. Feng, Z. Hussain, and Y. L. Chen, "A stable three-dimensional topological Dirac semimetal Cd_3As_2," Nat. Mater. **13**, 677–681 (2014).
[5] S. Borisenko, Q. Gibson, D. Evtushinsky, V. Zabolotnyy, B. Büchner, and R. J. Cava, "Experimental realization of a three-dimensional Dirac semimetal," Phys. Rev. Lett. **113**, 027603 (2014).
[6] M. Neupane, S.-Y. Xu, R. Sankar, N. Alidoust, G. Bian, C. Liu, I. Belopolski, T.-R. Chang, H.-T. Jeng, H. Lin, A. Bansil, F. Chou, and M. Z. Hasan, "Observation of a three-dimensional topological Dirac semimetal phase in high-mobility Cd_3As_2," Nat. Commun. **5**, 3786 (2014).
[7] T. Liang, Q. Gibson, M. N. Ali, M. Liu, R. J. Cava, and N. P. Ong, "Ultrahigh mobility and giant magnetoresistance in the Dirac semimetal Cd_3As_2," Nat. Mater. **14**, 280 (2015).
[8] S. M. Young, S. Zaheer, J. C. Y. Teo, C. L. Kane, E. J. Mele, and A. M. Rappe, "Dirac semimetal in three dimensions," Phys. Rev. Lett. **108**, 140405 (2012).
[9] B.-J. Yang and N. Nagaosa, "Classification of stable three-dimensional Dirac semimetals with nontrivial topology," Nat. Commun. **5**, 4898 (2014).
[10] A. A. Burkov, "Topological semimetals," Nat. Mater. **15**, 1145 (2016).
[11] X.-L. Qi and S.-C. Zhang, "Topological insulators and superconductors," Rev. Mod. Phys. **83**, 1057 (2011).
[12] H. Wang, H. Wang, H. Liu, H. Lu, W. Yang, S. Jia, X.-J. Liu, X. C. Xie, J. Wei, and J. Wang, "Observation of superconductivity induced by a point contact on 3D Dirac semimetal Cd_3As_2 crystals," Nat. Mater. **15**, 38 (2016).
[13] D. Samal, H. Nakamura, and H. Takagi, "Molecular beam epitaxy of three-dimensional Dirac material Sr_3PbO," APL Mater. **4**, 076101 (2016).
[14] Y. Kim, B. J. Wieder, C. L. Kane, and A. M. Rappe, "Dirac line nodes in inversion-symmetric crystals," Phys. Rev. Lett. **115**, 036806 (2015).
[15] R. Yu, H. Weng, Z. Fang, X. Dai, and X. Hu, "Topological node-line semimetal and Dirac semimetal state in antiperovskite Cu_3PdN," Phys. Rev. Lett. **115**, 036807 (2015).
[16] T. T. Heikkilä, N. B. Kopnin, and G. E. Volovik, "Flat bands in topological media," JETP Lett. **94**, 233 (2011).
[17] N. B. Kopnin, T. T. Heikkila, and G. E. Volovik, "High-temperature surface superconductivity in topological flat-band systems," Phys. Rev. B **83**, 220503 (2011).
[18] E. Tang and L. Fu, "Strain-induced partially flat band, helical snake states and interface superconductivity in topological crystalline insulators," Nat. Phys. **10**, 964 (2014).
[19] V. I. Iglovikov, F. Hébert, B. Grémaud, G. G. Batrouni, and R. T. Scalettar, "Superconducting transitions in flat-band systems," Phys. Rev. B **90**, 094506 (2014).
[20] H. Jacobs and U. Zachwieja, "Copper palladium nitride (Cu_3Pd_xN) with x = 0.020 and 0.989 as perovskites with the bound $3d^{10}$-$4d^{10}$ reciprocal effect," J. Less-Common Met. **170**, 185 (1991).
[21] R. Marchand, Y. Laurent, J. Guyader, P. L'Haridon, and P. Verdier, "Nitrides and oxynitrides: Preparation, crystal chemistry and properties," J. Eur. Ceram. Soc. **8**, 197 (1991).

[22] *The Chemistry of Transition Metal Carbides and Nitrides* , edited by S. T. Oyama (Blackie Academic & Professional, Glasgow, Scotland, 1996).
[23] D. D. Vaughn II, J. Araujo, P. Meduri, J. F. Callejas, M. A. Hickner, and R. E. Schaak, "Solution synthesis of Cu_3PdN nanocrystals as ternary metal nitride electrocatalysts for the oxygen reduction reaction," Chem. Mater. **26**, 6226 (2014).
[24] J. Jia, M. Shao, G. Wang, W. Deng, and Z. Wen, "Cu_3PdN nanocrystals electrocatalyst for formic acid oxidation," Electrochem. Commun. **71**, 61 (2016).
[25] T. Shiosaki, T. Yamamoto, T. Oda, and A. Kawabata, "Low-temperature growth of piezoelectric AlN film by rf reactive planar magnetron sputtering," Appl. Phys. Lett. **36**, 643 (1980).
[26] Lattice mismatch ε calculated as $\varepsilon = (a_{STO}\text{-}a_{film})/a_{film}$, where a_{STO} and afilm are the lattice constants of $SrTiO_3$ and Cu_3PdN, respectively.
[27] G. Koster, B. L. Kropman, G. J. H. M. Rijnders, D. H. A. Blank, and H. Rogalla, "Quasi-ideal strontiumtitanate crystal surfaces through formation of Sr-hydroxide,"Appl. Phys. Lett. **73**, 2920 (1998).
[28] SIMS analyses were performed by EAG Laboratories, Sunnyvale, CA.
[29] C. X. Quintela *et al.*, "Epitaxial CrN thin films with high thermoelectric figure of merit," Adv. Mater. **27**, 3032 (2015).
[30] W. Ramsay and S. Young, "The decomposition of ammonia by heat," J. Chem. Soc. Trans. **45**, 88 (1884).
[31] C. V. Thompson, "Structure evolution during processing of polycrystalline films," Annu. Rev. Mater. Sci. **30**, 159 (2000).
[32] U. Hahn and W. Weber, "Electronic structure and chemical-bonding mechanism of Cu_3N, Cu_3PdN, and related Cu(I) compounds," Phys. Rev. B **53**, 12684 (1996).
[33] M. Sieberer, S. Khmelevskyi, and P. Mohn, "Magnetic instability within the series TCu_3N (T = Pd, Rh, and Ru): A first-principles study," Phys. Rev. B **74**, 014416 (2006).
[34] M. G. Moreno-Armenta, W. L. Perez, and N. Takeuchi, "First-principle calculations of the structural and electronic properties of Cu_3MN compounds with M = Ni, Cu, Zn, Pd, Ag, and Cd," Solid State Sci. **9**, 166 (2007).
[35] E. H. Sondheimer and A. H. Wilson, "The theory of the magneto-resistance effects in metals," Proc. R. Soc. A **190**, 435 (1947).
[36] L. Wang, I. Gutierrez-Lezama, C. Berreteau, N. Ubrig, E. Giannini, and A. F. Morpurgo, "Tuning magnetotransport in a compensated semimetal at the atomic scale," Nat. Commun. **6**, 8892 (2015).
[37] P. Giannozzi *et al.*, "QUANTUM ESPRESSO: A modular and open-source software project for quantum simulations of materials," J. Phys.: Condens. Matter **21**, 395502 (2009).
[38] J. P. Perdew, K. Burke, and M. Ernzerhof, "Generalized gradient approximation made simple," Phys. Rev. Lett. **77**, 3865 (1996).
[39] L. Bellaiche and D. Vanderbilt, "Virtual crystal approximation revisited: Application to dielectric and piezoelectric properties of perovskites," Phys. Rev. B **61**, 7877 (2000).
[40] M. Sieberer, P. Mohn, and J. Redinger, "Role of carbon in $AlCNi_3$ and $GaCNi_3$: A density functional theory study," Phys. Rev. B **75**, 024431 (2007).
[41] D. F. Shao *et al.*, "Role of nitrogen in AlN_xMn_3: A density functional theory study," J. Appl. Phys. **113**, 023905 (2013).
[42] D. Kasugai, A. Ozawa, T. Inagaki, and K. Takenaka, "Effects of nitrogen deficiency on the magnetostructural properties of antiperovskite manganese nitrides," J. Appl. Phys. **111**, 07E314 (2012).
[43] X. Wang, J. Chen, and D. Xie, "Prospect of node-line semimetal Cu_3PdN to Be a topological superconductor," J. Supercond. Novel Magn. (published online).